A study of non-linearity in rainfall-runoff response using 120 UK catchments

Simon A. Mathias[a,*], Neil McIntyre[b], Rachel H. Oughton[a]

[a]*Department of Earth Sciences, Durham University, Durham, UK*
[b]*Centre for Water in the Minerals Industry, Sustainable Minerals Institute, The University of Queensland, Brisbane, Australia*

Abstract

This study presents a catchment characteristic sensitivity analysis concerning the non-linearity of rainfall-runoff response in 120 UK catchments. Two approaches were adopted. The first approach involved, for each catchment, regression of a power-law to flow rate gradient data for recession events only. This approach was referred to as the recession analysis (RA). The second approach involved calibrating a rainfall-runoff model to the full data set (both recession and non-recession events). The rainfall-runoff model was developed by combining a power-law stream-flow routing function with a one parameter probability distributed model (PDM) for soil moisture accounting. This approach was referred to as the rainfall-runoff model (RM). Step-wise linear regression was used to derive regionalization equations for the three parameters. An advantage of the RM approach is that it utilizes much more of the observed data. Results from the RM approach suggest that catchments with high base-flow and low annual precipitation tend to exhibit greater non-linearity in rainfall-runoff response. In contrast, the results from the RA approach suggest that non-linearity is linked to low evaporative demand. The difference in results is attributed to the aggregation of storm-flow and base-flow into a single system giving rise to a seemingly more non-linear response when applying the RM approach to catchments that exhibit a strongly dual

storm-flow base-flow response. The study also highlights the value and limitations in a regionalization context of aggregating storm-flow and base-flow pathways into a single non-linear routing function.

Keywords: Regionalization, Recession-slope curve, Ungauged catchments

1. Introduction

Rainfall-runoff modeling has long been recognized as an important methodology for improving our hydrological understanding of river catchments. Rainfall-runoff models are typically used to forecast river flow data for a given set of precipitation and potential evapotranspiration data (Wagener et al., 2001). Such models often have unknown model parameters that can be obtained by calibrating the models to observed river flow data (Wagener et al., 2001). For ungauged catchments (where no record of flow observations exist), model parameters can be estimated using regionalization relationships (Young, 2006).

Regionalization relationships are typically obtained by calibrating a rainfall-runoff model to multiple catchments and developing statistical relationships between the model parameters and non-flow data dependent parameters, often referred to as catchment characteristics (Young, 2006). Commonly used catchment characteristics include a range of different variables such as catchment area, soil-type, drainage path length, altitude and aridity (McIntyre et al., 2005; Young, 2006; Ye et al., 2014).

The efficacy of regionalization relationships is often compromised by inter-dependence between the model parameters themselves. This is because the inter-dependence increases the vari-

*Corresponding author. Tel.: +44 (0)1913343491, Fax: +44 (0)1913342301, E-mail address: s.a.mathias@durham.ac.uk

ance in the model parameter estimates. Furthermore it is difficult to develop a statistical relationship with catchment characteristics that maintains the complexity of the inter-dependence (McIntyre et al., 2005). These issues become worse with increasing number of model parameters. Various strategies have been proposed to manage these issues, including regionalization schemes that encompass the parameter inter-dependencies, or remove them, or screening of candidate rainfall-runoff model structures that achieve an acceptable balance between simplicity and capability (Lee et al., 2005).

Most rainfall-runoff models comprise at least two components (Wagener et al., 2001): (1) a soil moisture accounting process, used to calculate actual evapotranspiration and runoff generation; (2) a routing function, which transforms the runoff data into an estimate of flow rate at the catchment outlet. The soil moisture accounting process typically requires at least two model parameters, one for the capacity of the soil moisture store and another to help describe how actual evapotranspiration and runoff generation change as the catchment becomes progressively dryer (Lee et al., 2005). The routing function is commonly based on a network of stores each with a defined relationship between storage and outflow. Most commonly, at least when using daily rainfall-runoff data, the network comprises of two linear stores in parallel, conceptually representing the storm-flow and base-flow responses. This routing model requires three parameters: two residence times (one for each store) and a weighting factor defining the proportion of the runoff generation going to each store (Lee et al., 2005).

The perceived requirement of two residence times is often attributed to the existence of two modes of behavior: base-flow and storm-flow (Shaw et al., 2010; Beven, 2012). Base-flow is considered to be due to a slower acting set of hydrological pathways associated with subsurface

flow. Conversely, storm-flow is considered to be a faster component associated with flow through surface channel networks. From a calibration perspective, base-flow is required to satisfy the low flow rates observed during dry periods whereas storm-flow is required to simulate the high flow episodes that follow specific storm events.

Although conceptually simple, using a soil moisture store combined with two linear routing stores has had mixed success in terms of well-identified regionalization relationships. Challenges that have been encountered include the co-dependence of the weighting factor and the storm-flow residence time, and the high uncertainty in the base-flow residence time (Lee, 2006). Only using one non-linear routing store, with two parameters rather than three, is one approach to seeking a more identifiable regionalization relationship. A number of studies have demonstrated that a single non-linear store can match the performance of more complex routing functions in some types of gauged catchment (McIntyre, 2013).

The most commonly used non-linear routing store equation (e.g. Wittenberg, 1999; McIntyre et al., 2011; McIntyre, 2013; Ye et al., 2014) takes the form of a well established concept, that river flow can be approximated as a power law of the volume of water stored in the catchment, i.e. (Horton, 1945; Brutsaert and Nieber, 1977)

$$q = aV^b \tag{1}$$

were q [LT^{-1}] is the river flow rate per unit area of catchment, V [L] is the volume of water stored per unit area of catchment and a [$L^{1-b}T^{-1}$] and b [-] are empirical coefficients.

Considering overland sheet flow, Horton (1945) shows that under laminar conditions (using

Poiseuille's law) $b = 3$ and under turbulent conditions (using the Manning formula), $b = 5/3$. Alternatively, assuming that flow occurs through an unconfined aquifer, Brutsaert and Nieber (1977) show (using Darcy's law in conjunction with the Dupuit assumption, i.e., the Boussinesq equation) that $b = 2$.

The power law equation is commonly substituted into a mass conservation statement for the catchment. During recession periods (i.e., periods of negligible runoff generation), application of the chain-rule leads to a direct relationship between flow rate and the rate in change of flow rate

$$\frac{dq}{dt} = -\alpha q^{\beta} \tag{2}$$

where t [T] is time and α [$L^{1-\beta}T^{\beta-2}$] and β [-] can be found from:

$$\alpha = a^{1/b} b \quad \text{and} \quad \beta = \frac{2b-1}{b} \tag{3}$$

and the following inverse relationships apply:

$$a = [\alpha(2-\beta)]^{1/(2-\beta)} \quad \text{and} \quad b = \frac{1}{2-\beta} \tag{4}$$

Note, from Eq. (3), it can be seen that $\lim_{b\to\infty} \beta = 2$.

For a given set of discrete flow measurements, q_n [LT^{-1}], the coefficients α and β can be obtained by linear regression of an approximate form of Eq. (2) (Brutsaert and Nieber, 1977):

$$\ln\left(\frac{q_{n-1} - q_n}{t_n - t_{n-1}}\right) = \ln\alpha + \beta \ln\left(\frac{q_n + q_{n-1}}{2}\right) \tag{5}$$

The potential for reducing uncertainty in regionalization relationships makes the single non-linear store model a potentially attractive replacement for more complex routing models. However, there have been few empirical studies to explore how catchment characteristics control non-linearity in flow routing and whether the strength of these relationships permits a regional model to be proposed.

Ali et al. (2014) constructed a physically based hill-slope model to explore relationships between α, β and their physically based model parameters, by fitting Eq. (5) to results from multiple realizations of the physically based model. Step-wise linear regression analysis suggested that α and β were most sensitive to topographic slope, surface hydraulic conductivity, and the vertical exponential rate of decay for saturated hydraulic conductivity.

Ye et al. (2014) fitted Eq. (5) to recessions from daily flow data series from 50 river catchments from the eastern United States. They then provided a sensitivity analysis for α and β with respect to a range of different catchment characteristics including aridity index, drainage area, topographic slope, drainage density, soil water storage capacity, mean and standard deviation of surface saturated hydraulic conductivity and vertical exponential rate of decay for saturated hydraulic conductivity. It was found that α showed a strong sensitivity to a number of catchment characteristics including soil water storage capacity and surface saturated hydraulic conductivity. In contrast, β showed sensitivity only to aridity index and the rate of decay for saturated hydraulic conductivity.

The developed regression relationships of Ye et al. (2014) suggest that the non-linearity of catchment recession response increases with decreasing aridity and increasing soil hydraulic conductivity decline with depth. The highlighted importance of aridity here is cited as representing

an important inconsistency with the results obtained by studying the hill-slope model in the Ali et al. (2014) study.

A difficulty with the approach used by the Ye et al. (2014) study is that the application of Eq. (5) requires that much of the data set is ignored so as to ensure that all flow data used can be solely attributed to recession. Furthermore, there are many different methods available within the literature for excluding flow data in this way (e.g. Brutsaert and Nieber, 1977; Rupp and Selker, 2006; Kirchner, 2009), and these can lead to variations in α and β on the order of those expected by varying catchment characteristics (Stoelzle et al., 2013).

In this article 120 UK catchments, previously studied by McIntyre et al. (2005) and Young (2006), are revisited to further explore the role of catchment characteristics on non-linearity in rainfall-runoff response. This study builds on the existing work of Ye et al. (2014) by considering a broader range of catchment characteristics, commonly associated with the UK flood estimation handbook (Robson and Reed, 1999). A particular question arising with the UK data set is whether the lumping of storm- and base-flow responses into one conceptual store, as opposed to the conventional parallel stores used in the UK, can lead to meaningful relationships between parameters α and β and the CCs. While intuitively the answer is 'no', the lack of nationally available CCs describing hydrogeology means that regionalization of a base-flow residence time parameter is problematic anyway (Lee et al., 2005; Lee, 2006), and whether the recession and non-recession response can be modelled more holistically and parsimoniously on a national scale using the single non-linear store is therefore a valid question. Furthermore, to explore the impact of excluding non-recession data, two modelling approaches are adopted:

(1) Recession analysis. The first approach involves fitting Eq. (5) to recession data extracted

from each of the 120 UK catchments, analogous to Ye et al. (2014).

(2) Rainfall-runoff modelling. The second approach involves obtaining values of α and β by calibrating a rainfall-runoff model using Eq. (1) in conjunction with the so-called PDM soil moisture accounting procedure (Moore, 2007). The advantage of this second approach is that both recession and non-recession data are incorporated into estimates of α and β and it avoids arbitrary assumptions about when precipitation and evaporation can be neglected.

The structure of this article proceeds as follows. The sources of data for the 120 UK catchments are discussed. The relevant governing equations and methodologies associated with the two modelling approaches above are described in detail. Calibration, validation and regression results are presented for four selected catchments. Results from step-wise linear regression analysis for α and β with respect to the aforementioned catchment characteristics for all 120 catchments and for both modeling approaches are then presented and discussed.

2. Data and methodology

2.1. Data

The data used in this study represents 120 of the catchments previously presented by Young (2006). Each catchment contains a full set of daily precipitation, q_r [LT^{-1}], monthly Penman Monteith reference crop potential evaporation, E_p [LT^{-1}], and daily river flow data, q [LT^{-1}], for the period from 01/01/1979 to 31/12/1996. Statistical information regarding catchment characteristics of the catchments studied are presented in Table 1. Selected catchments represent a uniform coverage across the UK (consider Fig. 1 of Young (2006)), do not include any highly urbanised catchments, and represent (in a UK context) a broad range of altitudes and size.

River flow data were obtained from the UK National River Flow Archive maintained by the Centre for Ecology and Hydrology. Daily precipitation data were previously derived by Young (2006) for each catchment using the UK Meteorological Office daily precipitation library and a modified version of the Triangular Planes interpolation methodology (Young, 2006). Monthly averaged Penman Monteith reference crop potential evaporation was derived for each catchment from monthly averaged daily minimum and daily maximum temperature data from 1979 to 1996, also available from the UK Meteorological Office, using the method described in Example 20 of Allen et al. (1998). See Young (2006) for detail with regards to the derivation of the various catchment characteristics.

2.2. Recession analysis

Considering the various recession analysis methods discussed in the literature, including those of Brutsaert and Nieber (1977), Rupp and Selker (2006), Kirchner (2009) and Stoelzle et al. (2013), the following method was adopted and applied.

A set of flow rate gradient decline, J_m [LT^{-2}], corresponding flow rate, Q_m [LT^{-1}], and potential net precipitation (an estimate of the minimum possible net precipitation assuming actual evaporation = potential evaporation), $Q_{net,m}$, are obtained using the expressions (Brutsaert and Nieber, 1977):

$$J_m = \frac{q_{n-1} - q_n}{t_n - t_{n-1}} \tag{6}$$

$$Q_m = \frac{q_{n-1} + q_n}{2} \tag{7}$$

$$Q_{net,m} = \left(\frac{q_{r,n-1} + q_{r,n}}{2}\right) - \left(\frac{E_{p,n-1} + E_{p,n}}{2}\right) \quad (8)$$

where n denotes the n-th day in the time series of data.

Observations where $J_m < \omega$ (Rupp and Selker, 2006) and $Q_m < 10 \times Q_{net,m}$ (Kirchner, 2009) are excluded so as to ensure that only recession data are incorporated into the subsequent regression study, where ω is a threshold associated with numerical precision. Following the ideas presented by Rupp and Selker (2006), ω is set to five times the precision of the flow data for each catchment. In this study, the precision of each catchment data set is taken to be the minimum absolute non-zero value of J_m for each catchment. Values of α and β are then obtained by applying linear regression with Eq. (5). Regression is only applied to data from the period 1981 to 1991 to be consistent with the calibration period used in the rainfall-runoff modeling described below.

2.3. Rainfall-runoff modelling

A disadvantage of the above approach is that much of the high flow rate data is excluded due to its association with high net precipitation events. As discussed by Stoelzle et al. (2013), the data exclusion method adopted can strongly affect the derived values of α and β. To explore this further, α and β are re-estimated by calibrating a rainfall-runoff model to the entire set of flow data.

Following the work of McIntyre (2013), the non-linear routing function associated with Eq. (1) is coupled with a one parameter PDM soil moisture accounting procedure (Moore, 2007). The governing equations, solution procedures and calibration procedures are described below.

196 *2.3.1. Soil moisture accounting*

197 Let S [L] represent the total volume of water stored in soil across the catchment per unit area.
198 A mass conservation statement for S takes the form

$$\frac{dS}{dt} = q_r - E_a - q_{ro} - q_{in} - q_{vp} \tag{9}$$

199 where q_r [LT^{-1}], E_a [LT^{-1}], q_{ro} [LT^{-1}], q_{in} [LT^{-1}] and q_{vp} [LT^{-1}] are the rates of precipitation,
200 actual evapotranspiration, surface runoff, canopy interception and vertical percolation per unit
201 area, respectively.

202 The simplest possible model for E_a is to assume

$$E_a = \begin{cases} 0, & S = 0 \\ E_p, & S > 0 \end{cases} \tag{10}$$

203 In the past, many researchers have assumed that E_a/E_p increases linearly with S instead of Eq.
204 (10) (e.g. Chiew et al., 1993; Lamb and Kay, 2004; McIntyre et al., 2005; Lee et al., 2005; Moore,
205 2007). However, in this study it was found that Eq. (10) generally led to better model performance
206 (in terms of Λ, as calculated using Eq. (13)).

207 To determine how much runoff occurs, the so-call probability distributed model (PDM) of
208 Moore (2007) is imposed using a one parameter exponential distribution function. From the
209 derivation provided in Appendix A it is shown that

$$q_{ro} = \begin{cases} (S/S_{max})(q_r - q_{in}), & 0 \leq S < S_{max} \\ q_r - E_a - q_{in} - q_{vp}, & S = S_{max} \end{cases} \tag{11}$$

where S_{max} [L] is a calibration parameter, which represents both a maximum possible value of S and the mean local storage capacity within the catchment (assuming that local storage capacity is exponentially distributed across the catchment, see Appendix A).

Interception for woodland canopies is calculated using the interception model described by Gash et al. (1995), parameterized using the leafed and leafless canopy parameters obtained from Table 5 of Herbst et al. (2008). The proportion of woodland cover for each catchment is obtained from data provided by NRFA (2016). Following Sorensen et al. (2014), interception losses from non-woodland regions are ignored.

For simplicity, q_{vp} is assumed to be implicitly included in q_r. Furthermore, the time-lag associated with snow melt is assumed negligible (McIntyre et al., 2005; Young, 2006).

2.3.2. Runoff routing

The surface runoff, q_{ro}, is routed to the catchment outlet using the mass conservation statement

$$\frac{dV}{dt} = q_{ro} - q \tag{12}$$

where V [L] is the volume of water stored per unit area of catchment and q [LT^{-1}] is the river flow rate per unit area of catchment found from Eq. (1).

2.3.3. *Parameter estimation*

The above set of equations is solved using an Euler explicit time-stepping scheme as described in Appendix B. The resulting model has just three unknown parameters to be determined for each catchment including: α, b, S_{max}. It results in a more efficient optimisation of the parameters to find b as opposed to β because β has to be < 2 (recall Eq. (3)), whereas b is unconstrained.

Optimal parameter values are found by minimizing an objective function, Λ [-], found from

$$\Lambda = \left[\sum_{n=0}^{N} (\ln q_{o,n} - \ln q_{m,n})^2\right]\left[\sum_{n=0}^{N} \left(\ln q_{o,n} - \ln \overline{q}_{o,n}\right)^2\right]^{-1} \tag{13}$$

where N [-] are the number of data points in the calibration period, $q_{o,n}$ [LT^{-1}] is the observed flow data, $\overline{q}_{o,n}$ is the mean observed river flow rate for the calibration period and $\overline{q}_{m,n}$ is the simulated river flow rate data, using the rainfall-runoff model described above. Note that $(1 - \Lambda)$ represents the so-called Nash and Sutcliffe (1970) efficiency criterion for natural logs of discharge (hereafter referred to as NSE). It is appropriate to use logs here because of the special interest in river recession behavior.

Because there are only three unknown parameters, it is reasonable to use a local minimization algorithm. For this study, the local minimization routine FMINSEARCH, available in MATLAB, is used. Seed values adopted for all catchments when starting FMINSEARCH were 0.1 $mm^{1-\beta}day^{2-\beta}$, 1.0 and 10 mm for α, β and S_{max}, respectively.

The rainfall-runoff model is initialized with $S = S_{max}/2$ and $V = V_{max}/2$. Data used for calibration is taken from the period of 1981 to 1991. There is then a two year warm-up period, from 1979 to 1981. The remaining data, from 1991 to 1997, is used for validation purposes.

3. Results

3.1. Recession Analysis

Plots of observed flow rate gradient, J_m, against discharge rate, Q_m, are shown for four different catchments as green dots in Fig. 1. These example catchments are chosen to represent a range of catchment types in terms of the expected base-flow index, BFIHOST, and average annual rainfall, SAAR. Subplots a) and d) show results for catchments with low and high BFIHOST, respectively (see Table 2 for actual values of BFIHOST). Subplots b) and c) show catchments with intermediate values of BFIHOST. Subplots a) and c) show results for catchments with high SAAR. Subplots b) and d) show results for catchments with relatively low SAAR. While these four examples provide a limited sample of the range of hydrological responses over all 120 catchments, they provide a useful representation of the type of results obtained from the wider analysis.

Large values of BFIHOST indicate catchments with a large groundwater component. Groundwater catchments tend to have relatively larger summer flows and are less responsive to individual precipitation events, and hence have lower maximum flows, as compared to surface water dominated catchments. This is clearly indicated by comparing Figs. 1 a) and d).

The red dots shown in Fig. 1 represent those events that have been classified as recession events (i.e., $J_m \geq \omega$ and $Q_m \geq 10 \times Q_{net,m}$). It is clear that these rules eliminate the majority of the data. Furthermore, the selected recession data do not contain the higher Q_m ranges. The red solid straight lines result from fitting Eq. (5) to the recession data using linear regression, hereafter referred to as the recession analysis (RA).

As a first attempt to understand how the fitting parameters are controlled by catchment char-

acteristics (CC), the following study was conducted using the cumulative distribution functions (CDF) of α and β resulting from RA for each of the 120 catchments.

Note that SPRHOST was excluded from the analysis because it was found to be strongly correlated with BFIHOST (i.e., had a correlation coefficient, $|R| > 0.9$). Similarly, DPLBAR and LDP were excluded because they were found to be strongly correlated with AREA (i.e., had correlation coefficients, $|R| > 0.9$). Furthermore, ALTBAR and DPSBAR were excluded because they were found to be strongly correlated with SAAR (i.e., had correlation coefficients, $|R| > 0.7$). Although this step avoided highly correlated pairs of CCs, a number of significant correlations between CCs remain that will be considered when interpreting the physical controls on non-linearity. The correlation coefficients between the CCs discussed above are presented for reference in Table 3.

Each of the retained CCs in Table 1 was ranked (from lowest to highest CC value) for the 120 catchments and separated out into lower, middle and higher third sub-samples. CDFs for α and β were then constructed using the catchments corresponding to each of the three thirds for each of the CCs. The Kolmogorov–Smirnov (KS) statistic (Ang and Tang, 1975, p. 277–280) was assessed for each of the CCs by measuring the maximum difference between the CDFs of the lower and upper third sub-samples. The CCs were then ranked in terms of KS for both the α and β CDFs. Those CCs that exhibit high KS values can be viewed as having a greater control over the distribution of values of α and/or β.

Figs. 2a, b and c show the CDFs for the three most sensitive CCs in terms of α from the RA. Figs. 2d, e and f show the CDFs for the three most sensitive CCs in terms of β from the RA. The associated KS values are provided in brackets alongside the x-axis labels.

The results suggest that α is most sensitive to BFIHOST, URBEXT and FARL. Most of the

sensitivity appears to be due to BFIHOST. The high BFIHOST catchments correspond to low α values. When $\beta = 1$, α can be thought of as the reciprocal of a residence time for a catchment. The results therefore suggest that high BFIHOST corresponds to higher residence times, which one would expect.

The dependence on FARL can be explained in a similar manner: FARL is an index of flood attenuation due to lakes and reservoirs, where catchments with larger values of FARL have fewer lakes and reservoirs connected to the stream network. Therefore, higher values of FARL tend to have lower residence times, equivalent to higher values of α, as shown in Figure 2c. Figure 2b shows that more urbanised catchments are associated with higher residence times. This may be explained by the fact that urbanised catchments tend to have lower FARL values due to artificial storage (the URBEXT-FARL correlation in Table 3 is -0.4) leading to longer residence times. Furthermore, highly urbanised catchments have been excluded from the dataset, so the strong independent effect of urbanisation on flow residence time, which would tend to reduce residence times, is not seen in this analysis.

For β, the largest values correspond to low PEANN, low URBEXT and high AREA. The idea that low evaporation and high precipitation leads to greater non-linearity is consistent with the finding of Ye et al. (2014) that β decreases with increasing aridity. The dependence of URBEXT mirrors the dependence on PEANN, which is likely to be due to the correlation between these two CCs (Table 1) rather than any independent effect of URBEXT. For catchments with large areas, there is a greater likelihood of a storm-flow recession being superimposed on a base-flow recession. This would cause periods of steeper recessions to be included, and so may explain the increasing β values with increasing AREA.

It is also interesting to note from Fig. 2 that the regression analysis of recession data has led to the estimation of β values greater than 2 for several catchments, leading to negative values of b (recall Eq. (4)), which is physically unrealistic. Also, Fig. 2 shows that the higher range of PEANN catchments do not lead to linear responses, but to β values less than 1.0. This is not consistent with the values of β applicable to idealised hydrological systems, and is likely to be due to flood plain storage in low slope catchments (PEANN is negatively correlated with DPSBAR, $R = -0.44$).

Regionalization equations were also constructed using step-wise linear regression. Following one of the approaches adopted by Ye et al. (2014), additional parameters were added until the so-called Bayesian Information Criterion (BIC) (i.e., Eq. (12) of Ye et al. (2014)) was minimized. Catchments with $\beta \geq 2$ were excluded from this process.

The step-wise linear regression procedure used can be described in more details as follows: (1) determine the correlation coefficients of each CC with the parameter of concern (α, β etc.); (2) select the CC with the highest absolute correlation coefficient; (3) develop a linear regression relationship between this plus any previously selected CC(s) and the parameter of concern; (4) calculate the BIC; (5) determine the correlation coefficients of the remaining CCs with the residuals between the developing regionalization relationship and the parameter of concern; (6) repeat steps 2 to 4; (7) if the new BIC is less than the previous BIC repeat steps 5 to 7, otherwise consider the current form of the regionalization relationship to be optimal.

The resulting regionalization equations took the form:

$$\alpha = \frac{0.8014\ \mathrm{AREA}^{-0.1788}}{\exp(3.792\ \mathrm{BFIHOST})} \tag{14}$$

$$\beta = \frac{13.53\ \mathrm{AREA}^{0.08887}}{\exp(0.00492\ \mathrm{PEANN} + 0.6063\ \mathrm{BFIHOST})} \tag{15}$$

which had correlation coefficients, R, of 0.78 and 0.62, respectively. The most sensitive CCs identified in Fig. 2 (i.e., BFIHOST for α and PEANN for β) are present in Eqs. (14) and (15). But the regionalization equations also elude to a high dependency of α on AREA and a high dependency of β on BFIHOST. Of particular note is the absence of URBEXT from both Eqs. (14) and (15).

For comparison, the recession lines resulting from Eqs. (14) and (15) are displayed for each of the four example catchments shown in Fig. 1 as red dashed lines. The comparison between the regionalization and original recession models is less favorable in Figs. 1b and d.

3.2. Rainfall-runoff modeling

Also shown, as black solid straight lines in Fig. 1, are the recession lines derived by calibrating the aforementioned rainfall-runoff model to the full set of flow data, during the calibration period (1981 to 1991), hereafter referred to as the rainfall-runoff modeling (RM). Recession lines in these examples and from RM in general are much steeper than those generated by RA (the red solid straight lines, as discussed in the previous section). Steeper gradients imply higher β values (recall Eq. (5)). Incorporating the higher discharge rate data, associated with non-recession events, generally leads to a more non-linear models. At the same time, using the RM limits the beta

values to be physically consistent with the single store model and hence eliminates the previously mentioned instances where $\beta \geq 2$.

Fig. 3 shows time-series plots of flow for the four catchments previously presented in Fig. 1. Note that the time-period shown includes only the validation period (1991 to 1997). The observed data are presented as a green thick line. The results from the calibrated rainfall-runoff models are presented as blue lines. Relevant parameter values along with NSE values for both calibration and validation periods are presented in Table 2.

The four catchments represent examples of quite different rainfall-runoff response. It is clear that the three-parameter rainfall-runoff model is able to capture many aspects of the flow dynamics, beyond just the recession events, for a range different BFIHOST values. However, the model tends to underestimate the peak flow rates, although this latter point may be more to do with the fact that we are using daily as opposed to (say) hourly precipitation data (Wang et al., 2009). The model is also poor at predicting significant flow events during the summer periods for catchment b) (i.e., Fig. 3b), which represents a relatively dry catchment with only a moderate fraction of base-flow (recall Table 2).

Figs. 4a, b and c show the CDFs for the top three most sensitive CCs in terms of α derived from RM. Figs. 4d, e and f show the CDFs for the top three most sensitive CCs in terms of β derived from RM. Figs. 4g, h and i show the CDFs for the top three most sensitive CCs in terms of the PDM parameter, S_{max}, derived from RM. Again, the associated KS values are provided in brackets alongside the x-axis labels.

As with the RA results presented in Fig. 2a, it is clear from Fig. 4a that higher BFIHOST leads to lower α values. Something that is uncommon to the RA results presented in Fig. 2

however, is that for the RM results, β shows a strong dependence on BFIHOST as well, with low BFIHOST leading to a more linear response (see Fig. 4d). It is also found that β is smaller for wetter catchments (i.e., high SAAR). However, it is also clear from Fig. 4 that β becomes largely insensitive to BFIHOST when BFIHOST > 0.433 and largely insensitive to SAAR when SAAR < 1151 mm.

From Figs. 4g, h and i, it can be seen that the lowest S_{max} values are found in catchments with high precipitation (high SAAR), low evaporation (low PEANN) and close to zero urban extent (i.e., URBEXT < 0.0015), which is consistent with other regionalisation studies (Lee et al., 2006; Kjeldsen et al., 2005).

The results in Fig. 4 are difficult to interpret without looking in more detail at the distribution of the parameter values and their relationships with each other and CCs. Hence, to explore rainfall-runoff model parameter sensitivity further, a series of univariate plots are presented in Fig. 5. There are reasonably high levels of correlation between α and BFIHOST as well as of S_{max} with SAAR and PEANN (Figs. 5a,d and e). In contrast, the correlation between β and its two most sensitive CCs, BFIHOST and SAAR is quite weak (Figs. 5b and c). From Figs. 5g and h it is clear that there is very little cross-correlation between α and S_{max} as well as β and S_{max}. However, in Fig. 5i it can be seen that the correlation coefficient between β and α is relatively high (as compared to correlation with CCs) at -0.532. For comparison, the correlation coefficient between β and α values obtained from the recession analysis in the previous section was just -0.0095.

Fig. 4 shows that many β values are close to the plausible maximum of 2.0 and considerably higher than values estimated for idealised hydrological systems. This indicates the widespread presence of wetness thresholds at which the flow velocities increase markedly, which includes

388 the transition from base-flow dominated to storm-flow dominated flows in catchments where both
389 modes exist. This would partially explain why uni-modal catchments, with either very high or
390 very low BFIHOST values, tend to have lower β values (Fig. 5b).

391 In the same way as described in the previous sub-section, regionalization equations were also
392 derived for α, b (β does not lend itself to regression here because so many values are close to the
393 constraint of 2, therefore b was used instead) and S_{max} from the RM data. These were as follows:

$$\alpha = \frac{0.4533}{\text{BFIHOST}^{1.758}\ \text{SAAR}^{0.4683}} \tag{16}$$

$$\beta = 2 - \frac{4.581 \times 10^{-7}\ \text{SAAR}^{1.569}}{\text{BFIHOST}^{0.9324}} \tag{17}$$

$$S_{max} = \frac{\text{PEANN}^{5.519} \exp(13.71\ \text{FARL} + 0.0004602\ \text{SAAR})}{1.377 \times 10^{-11}\ \text{SAAR}^{2.617} \exp(4.295\ \text{DPLCV})} \tag{18}$$

394 which have correlation coefficients, R, of 0.7310, 0.4979 and 0.7930, respectively. Note that the
395 regionalization equation for b is written instead for β by virtue of Eq. (3) (see Eq. (17)).

396 For comparison, the recession lines resulting from Eqs. (16) and (17) are displayed for each of
397 the four example catchments shown in Fig. 1 as dashed black lines.

398 Fig. 3 shows as redlines, flow predictions during the validation period using the rainfall-
399 runoff model with α, β and S_{max} calculated using Eqs. (16) to (18). From the provided validation
400 and regionalization NSE values for the four catchments given in Table 2, it is apparent that the
401 regionalization relationships are almost as effective as model calibration in terms of predicting

flow data at the four catchments studied. Considering the NSE values for all 120 catchments shows the generally small loss of performance when moving from using calibrated to regionalised parameters, for example the respective median NSE values across all 120 catchments are 0.79 and 0.75.

Fig. 6 shows how NSE values from the calibration period, the validation period with the calibration parameters and the validation period using the regionalization equations, Eqs. (16) to (18), vary with the most sensitive CCs. For all three sets of NSE values, it is found that the best performing models are in catchments with high precipitation (high SAAR). NSE values are not found to be that sensitive to other CCs.

3.3. Comparison of RA and RM methods

The plots of BFIHOST against SAAR and PEANN against AREA in Fig. 7 have been constructed to further illustrate how β values and model performance vary over the associated parameter space. Figs. 7a and d were constructed as follows. The 120 catchments were ranked according to β values obtained from the RA method and then split into three groups with equal number of catchments. The green, blue and red markers in Figs. 7a and d represent those catchments in groups with the lowest, intermediate and highest values of β, respectively (as indicated by the legend). The plots in Figs. 7b and e were constructed in an identical way except using β values from the RM method. Figs. 7c and f were also constructed in the same way except using NSE values from the RM method during the validation period (as opposed to β values).

From Figs. 7a and b, it is apparent that both the RA and RM method lead to the highest β values in catchments with relatively low rainfall (500 mm < SAAR < 1500 mm) and moderate

Table 1: Minimum, mean and maximum values of the catchment characteristics for 120 catchments studied. Definitions are from Robson and Reed (1999) and Young (2006).

Abbreviations	Definitions	min.	mean	max.
ALTBAR	Mean catchment altitude (m above sea level).	38	215	557
AREA	Catchment drainage area (km^2).	1.1	271	1700
ASPBAR	Index representing the dominant aspect of catchment slopes (mean aspect, clock wise 0-360^o).	0.8	144	359
ASPVAR	Index describing the invariability in aspect of catchment slopes.	0.02	0.192	0.513
BFIHOST	Base-flow index derived using the HOST classification.	0.238	0.496	0.937
DPLBAR	Index describing catchment size and drainage path configuration (km).	1.14	18.6	57.62
DPLCV	Coefficient of variation of the drainage network distances.	0.332	0.435	0.606
DPSBAR	Index of catchment steepness (m/km).	13	97	306
FARL	Index of flood attenuation due to reservoirs and lakes.	0.92	0.99	1.00
LDP	Longest drainage path (km).	2.7	35.0	121
PEANN	1961-1990 standard period average annual potential evaporation (mm).	461	549	654
SAAR	1941-1970 standard period average annual rainfall (mm).	602	1093	2860
SPRHOST	SPR (standard percentage runoff) derived using the HOST classification.	6.9	37.4	58.3
URBEXT	FEH index of fractional urban extent	0	0.010	0.127

quantities of base-flow ($0.3 < \text{BFIHOST} < 0.7$). Also shown as black dots are those catchments that had β values ≥ 2 (recall this only occurs using the RA method), which are also mostly located in this region. From Fig. 7c it can be seen that most of those catchments that scored relatively low NSE values from the RM method during the validation period are also located in this low SAAR and medium-range BFIHOST region.

A medium-range BFIHOST is indicative of a catchment with both strong base-flow and storm-flow components (e.g., consider Figs. 3b and c). Arguably, a high β value is likely to arise

Table 2: Some details concerning the catchments used for the results presented in Figs. 1 and 3. Catchments a), b), c) and d) are the catchments used to get the results in Figs. 1a, b, c, d and 3a, b, c, d, respectively. The α, β, S_{max} are parameters values obtained by calibrating the rainfall-runoff model to the flow data. Calibration NSE, Validation NSE and Regionalization NSE are Nash-Sutcliffe efficiency values obtained during the calibration period, the validation period using the calibrated parameters and the validation period using the regionalization relationships, respectively.

Catchment	a)	b)	c)	d)
Gauge number	80001	54018	55014	43005
AREA (km^2)	197	170	203	326
BFIHOST	0.376	0.504	0.593	0.903
SAAR (mm)	1352	780	1062	768
PEANN (mm)	507	543	549	592
URBEXT	0.00040	0.00490	0.00230	0.01540
α ($mm^{1-\beta}day^{\beta-2}$)	0.114	0.091	0.032	0.016
β	1.681	1.976	1.985	1.799
S_{max} (mm)	35.39	83.97	48.89	62.38
Calibration NSE	0.905	0.855	0.902	0.905
Validation NSE	0.898	0.845	0.923	0.921
Regionalization NSE	0.767	0.794	0.867	0.886

from such a catchment due to the forcing of this strongly dual-modal hydrological response to be represented by a single non-linear store. The results presented in Figs. 7 a and b suggest that this is particularly the case for dryer catchments (i.e., low SAAR). Furthermore, the low NSE values, associated with low SAAR and medium-range BFIHOST, in Fig. 7 c provides strong evidence that a single non-linear store is not suitable for regionalization in this subset of catchments.

In Fig. 7d (and also Fig. 2d), it is apparent that high evaporative demand (i.e., high PEANN) leads to lower β values when considering the RA method. Consistent with this, Ye et al. (2014) found lower values of β to occur in flatter catchments with high aridity index. As discussed earlier, there is a moderately negative correlation between evaporative demand and steepness of a catchment.

Fig. 7e and previous results show that many of the β values estimated using the RM method

Table 3: Correlation coefficients, *R*, for the catchment characteristics. See Table 1 for catchment characteristic definitions.

	ALTBAR	AREA	ASPBAR	ASPVAR	BFIHOST	DPLBAR	DPLCV	DPSBAR	FARL	LDP	PEANN	SAAR	SPRHOST	URBEXT
ALTBAR	1.0	0.1	-0.1	0.2	-0.5	0.1	0.2	**0.7**	0.2	0.1	-0.6	**0.7**	0.5	-0.4
AREA	0.1	1.0	-0.2	-0.4	0.1	**0.9**	0.1	0.1	-0.1	**0.9**	-0.3	-0.1	0.0	-0.1
ASPBAR	-0.1	-0.2	1.0	-0.1	0.0	-0.2	0.1	-0.1	0.1	-0.2	0.2	0.0	0.1	-0.1
ASPVAR	0.2	-0.4	-0.1	1.0	-0.2	-0.5	0.1	0.1	0.1	-0.5	0.1	0.2	0.1	0.1
BFIHOST	-0.5	0.1	0.0	-0.2	1.0	0.1	-0.2	-0.2	-0.1	0.1	0.4	-0.4	**-0.9**	0.1
DPLBAR	0.1	**0.9**	-0.2	-0.5	0.1	1.0	0.1	0.0	-0.2	**1.0**	-0.3	-0.2	-0.1	-0.1
DPLCV	0.2	0.1	0.1	0.1	-0.2	0.1	1.0	0.1	0.2	0.2	-0.1	0.2	0.2	-0.2
DPSBAR	**0.7**	0.1	-0.1	0.1	-0.2	0.0	0.1	1.0	0.2	0.0	-0.4	**0.8**	0.3	-0.4
FARL	0.2	-0.1	0.1	0.1	-0.1	-0.2	0.2	0.2	1.0	-0.2	0.1	0.1	0.1	-0.4
LDP	0.1	**0.9**	-0.2	-0.5	0.1	**1.0**	0.2	0.0	-0.2	1.0	-0.3	-0.1	-0.1	-0.1
PEANN	-0.6	-0.3	0.2	0.1	0.4	-0.3	-0.1	-0.4	0.1	-0.3	1.0	-0.3	-0.5	0.3
SAAR	**0.7**	-0.1	0.0	0.2	-0.4	-0.2	0.2	**0.8**	0.1	-0.1	-0.3	1.0	0.5	-0.2
SPRHOST	0.5	0.0	0.1	0.1	**-0.9**	-0.1	0.2	0.3	0.1	-0.1	-0.5	0.5	1.0	-0.2
URBEXT	-0.4	-0.1	-0.1	0.1	0.1	-0.1	-0.2	-0.4	-0.4	-0.1	0.3	-0.2	-0.2	1.0

are close to the physically plausible upper bound value of 2.0. This result is likely to be due to the β parameter's role in fitting the rising limb and peak of the hydrograph as well as the recessions, rather than strong non-linearity in either of these parts of the hydrograph. The highest β values tend to be in catchments with medium to high evaporative demand, which tend to have medium to high BFIHOST values, and also catchments with lower areas. We speculate that this is due to the presence of high flow peaks as well as strong base-flow responses in these types of catchment; while in catchments with very high or low values of BFIHOST and/or with larger areas, there are simpler responses and/or more potential for smoothing and spatial integration of flow signals upstream of gauging stations. Therefore, while the use of the parsimonious, 3-parameter

rainfall-runoff method may be valuable for regionalisation across some types of catchments and utilises much more of the rainfall-runoff data, interpretation of the β parameter in terms of physical processes is arguably better approached using the RA method.

4. Summary and conclusions

The objective of this study was to explore the role of catchment characteristics on non-linearity in rainfall-runoff response using daily precipitation, potential evapotranspiration and river flow data from 120 UK river catchments. Two approaches were taken for estimating the power-law parameters α and β describing the degree of apparent non-linearity in the catchments: The first approach involved regression of a power-law to flow rate gradient data for recession events only. Recession events were identified as those where the flow rate was greater than ten times the precipitation minus the potential evapotranspiration. Recession events with flow rate gradients less than five times the precision of the flow data were excluded. This approach was referred to as the recession analysis (RA). The second approach involved calibrating a rainfall-runoff model to the full data set (both recession and non-recession events). The rainfall-runoff model was developed by combining a power-law streamflow routing function with a one parameter probability distributed model (PDM) for soil moisture accounting. This approach was referred to as the rainfall-runoff model (RM). The dependency of the estimated parameters on CCs was evaluated by looking at how strongly the parameter values changed between three ranges of each CC, and also by applying step-wise linear regression.

The RA approach suggests that β values are most sensitive to evaporative demand, with lower potential evaporation causing higher β values and thus greater non-linearity. This result is similar

to that found by Ye et al. (2014) following their application of RA to 50 catchments in the USA. Specifically, Ye et al. (2014) found that lower aridity index led to higher values of β (see their Eq. 14b). Catchments (from the current study) with high potential evaporation often had β values less than one, signifying that recession rates become faster as these catchments become drier, which may be related to flood plain activation in wetter conditions.

The RM approach led to contrasting results, with generally much higher β values, and with high base-flow, low rainfall, high potential evaporation catchments tending to cause the highest β values. The higher β values are likely to be because β has a role in enabling the rainfall-runoff model to match the high flows as well as the base-flows, especially in catchments where base-flow is significant but the model still struggles to match peak flows (e.g. Fig. 3d). Despite using a relatively parsimonious rainfall-runoff model, with only three parameters, the RM approach suffered more than the RA approach in terms of covariance between the α and β values. Its general performance on test catchments in terms of the NSE value is comparable to those achieved by regionalisation of less parsimonious models (McIntyre et al., 2005; Lee et al., 2006) (noting that the comparison is not direct because these other studies did not log-transform the flows prior to calculating the NSE).

In conclusion, while there may be value in refining the 3-parameter rainfall-runoff model and exploring applicability further, the 2-parameter recession analysis gave values of β that have lower covariance, are more physically plausible and interpretable in terms of the CCs, and are explained better by the CCs in terms of regression correlation coefficient. The recession analysis found that catchments with low evaporative demand exhibit greater non-linearity, with values of β more consistent with theoretical values for idealized catchments, while dryer catchments have β values

close to one on average, but with wide variation around this value. This new knowledge of controls on non-linear recession behavior has potential value in improving regionalization of base-flow responses, which has consistently been a problem across UK catchments (Lee et al., 2006).

5. Acknowledgements

We are very grateful for the useful comments provided by an anonymous reviewer from the Journal of Hydrology.

6. References

Ali, M., Ye, S., Li, H. Y., Huang, M., Leung, L. R., Fiori, A., and Sivapalan, M. (2014), Regionalization of subsurface stormflow parameters of hydrologic models: Up-scaling from physically based numerical simulations at hillslope scale, J. Hydrol., 519, 683–698.

Allen, R. G., Pereira, L. S., Raes D., Smith M. (1998), Crop evapotranspiration-guidelines for computing crop water requirements. In FAO Irrigation and drainage, Paper 56, Rome.

Ang, A. H. S. and Tang, W. H. (1975), robability concepts in engineering planning and design. Vol. 1basic principles. Wiley, New York.

Beven, K. J. (2012), Rainfall-Runoff Modelling: The Primer, Second Edition, John Wiley & Sons.

Brutsaert, W., and Nieber, J. L. (1977), Regionalized drought flow hydrographs from a mature glaciated plateau, Water Resour. Res., 13, 637–643.

Chiew, F. H. S., Stewardson, M. J., McMahon, T. A. (1993), Comparison of six rainfall-runoff modelling approaches, J. Hydrol., 144, 1–36.

Gash, J. H. C., Lloyd, C. R., Lachaud, G. (1995), Estimating sparse forest rainfall interception with an analytical model, J. Hydrol., 170, 79–86.

Herbst M., Rosier P. T. W., McNeil D. D., Harding R. J., Gowing D. J. (2008), Seasonal variability of interception evaporation from the canopy of a mixed deciduous forest, Agricultural and Forest Meteorology, 148, 1655–1667.

Horton, R. E. (1945), Erosional development of streams and their drainage basins; hydrophysical approach to quantitative morphology, Geol. Soc. Am. Bull., 56, 275–370.

Kirchner, J. W. (2009), Catchments as simple dynamical systems: Catchment characterization, rainfall-runoff modeling, and doing hydrology backward, Water Resour. Res., 44, W02429.

Kjeldsen, T. R., Stewart, E. J., Packman, J. C., Folwell, S. S. and Bayliss, A. C. (2005), Revitalisation of the FSR/FEH Rainfall Runoff Method, R&D Technical Report FD1913/TR, Department for Environment, Food and Rural Affairs, London.

Lee, H., McIntyre, N., Wheater, H., and Young, A. (2005), Selection of conceptual models for regionalisation of the rainfall-runoff relationship, J. Hydrol., 312, 125–147.

Lamb, R., Kay, A. L. (2004),Confidence intervals for a spatially generalized, continuous flood frequency model for Great Britain, Water Resour. Res., 40, W07501.

Lee, H. (2006), Regionalisation of Rainfall-Runoff Models in the UK, PhD Dissertation, Imperial College London.

Lee, H., McIntyre, N., Wheater, H., and Young, A. (2006), Predicting runoff in ungauged UK catchments, Proceedings of the Institution of Civil Engineers-Water Management, 159, 129–138.

McIntyre, N., Lee, H., Wheater, H., Young, A., and Wagener, T. (2005), Ensemble predictions of runoff in ungauged catchments, Water Resour. Res., 41, W12434.

McIntyre, N., Young, P., Orellana, B., Marshall, M., Reynolds, B., and Wheater, H. (2011), Identification of nonlinearity in rainfall-flow response using data-based mechanistic modeling, Water Resour. Res., 47, W12434.

McIntyre, N. (2013), Apportioning non-linearity in conceptual rainfallrunoff models: examples from upland UK catchments, Hydrol. Res., 44.6, 965–981.

Moore, R. J. (2007), The PDM rainfall-runoff model, Hydrol. Earth Syst. Sci., 6, 483–499.

Nash, J., & Sutcliffe, J. V. (1970), River flow forecasting through conceptual models part IA discussion of principles, Journal of Hydrology, 10, 282–290.

NRFA (2016), National River Flow Archive, http://nrfa.ceh.ac.uk/data/search, Accessed 25/04/2016.

Robson, A., Reed, D.W. (1999), Statistical Procedures for Flow Frequency Estimation. Flood Estimation Handbook Vol.3, NERC, Wallingford.

Rupp, D. E., and Selker, J. S. (2006), Information, artifacts, and noise in dQ/dt - Q recession analysis, Adv. Water Resour., 29, 154–160.

Shaw, E. M., Beven, K. J., Chappell, N. A., and Lamb, R. (2010), Hydrology in Practice, Fourth Edition, CRC Press.

Sorensen, J. P. R., Finch, J. W., Ireson, A. M., Jackson, C. R. (2014), Comparison of varied complexity models simulating recharge at the field scale, Hydrol. Process., 28, 2091–2102.

Stoelzle, M., Stahl, K., and Weiler, M. (2013), Are streamflow recession characteristics really characteristic?, Hydrol. Earth Syst. Sci., 17, 817–828.

Ye, S., Li, H. Y., Huang, M., Ali, M., Leng, G., Leung, L. R., Wang, S. Q., and Sivapalan, M. (2014), Regionalization of subsurface stormflow parameters of hydrologic models: Derivation from regional analysis of streamflow recession curves, J. Hydrol., 519, 670–682.

Young, A. R. (2006), Stream flow simulation within UK ungauged catchments using a daily rainfall-runoff model, J. Hydrol., 320, 155–172.

Wagener, T., Boyle, D. P., Lees, M. J., Wheater, H. S., Gupta, H. V., and Sorooshian, S. (2001), A framework for development and application of hydrological models, Hydrol. Earth Syst. Sci., 5, 13–26.

Wang, Y. I., He, B. I. N., and Takase, K. (2009), Effects of temporal resolution on hydrological model parameters and its impact on prediction of river discharge, Hydrol. Sci. J., 54, 886–898.

Wittenberg, H. (1999), Baseflow recession and recharge as nonlinear storage processes, Hydrol. Process., 13, 715–726.

Appendix A. The probability distributed model (PDM)

Building on work presented by Moore (2007), below is an explanation of the probability distributed model (PDM) for relating the rate of runoff, q_{ro} [LT^{-1}], with the volume of water stored in soil across the catchment per unit area, S [L].

Let A [L^2] be the area of the catchment. At any given time, a portion of this area, A_c [L^2], contains water-logged land surface such that additional precipitation leads to the generation of

runoff. Moore (2007) considers the soil storage capacity at any point within the catchment, c [L], to be a random variable defined by a probability density function, $f(c)$ [L^{-1}]. Let C [L] be the maximum value of c observed within the area A_c. It can then be stated that $A_c = F(C)A$ where $F(C)$ [-] is the probability of c not exceeding C, defined as

$$F(C) = \int_0^C f(c)dc \tag{A.1}$$

Moore (2007) further argues that the rate of runoff, q_{ro} [LT^{-1}], can therefore be estimated from

$$q_{ro} = F(C)(q_r - q_{in}) \tag{A.2}$$

where q_r [LT^{-1}] and q_{in} [LT^{-1}] are the rates of precipitation and canopy interception, respectively.

The water storage level within the catchment is equal to c in the water-logged regions and assumed to be equal to C outside of these regions. It follows that S can be calculated from (Moore, 2007)

$$S = \int_0^C c f(c)dc + C\int_C^\infty f(c) = \int_0^C (1 - F(c))dc \tag{A.3}$$

If c conforms to a single parameter exponential distribution, the $F(c)$ function takes the form (Moore, 2007)

$$F(c) = 1 - \exp\left(-\frac{c}{\bar{c}}\right) \tag{A.4}$$

where $\bar{c}$ [L] represents the mean local storage capacity within the catchment.

578 Substituting Eq. (A.4) into Eq. (A.3) leads to

$$S = \bar{c}\left[1 - \exp\left(-\frac{C}{\bar{c}}\right)\right] = \bar{c}F(C) \tag{A.5}$$

579 from which it is noted that the maximum possible value of S, S_{max}, is found from

$$S_{max} = \bar{c} \tag{A.6}$$

580 and from Eq. (A.2), that

$$q_{ro} = \frac{S}{S_{max}}(q_r - q_{in}), \quad 0 \le S < S_{max} \tag{A.7}$$

581 **Appendix B. Details of the Euler explicit time-stepping scheme**

582 The set of equations described in Section 2.3 are solved using an Euler explicit time-stepping

583 scheme. In this way, it can be said from Eqs. (9) and (12) that

$$S_{n+1} = S_n + \Delta t(q_{r,n} - E_{a,n} - q_{ro,n} - q_{in,n} - q_{vp,n}) \tag{B.1}$$

$$V_{n+1} = V_n + \Delta t(q_{ro,n} - q_n) \tag{B.2}$$

584 From Appendix C below it can be seen that stability of the scheme is ensured providing

$$\frac{\partial}{\partial S}\left(-q_r + E_a + q_{ro} + q_{in} + q_{vp}\right) < \frac{1}{\Delta t} \tag{B.3}$$

$$\frac{\partial}{\partial V}(-q_{ro} + q) < \frac{1}{\Delta t} \tag{B.4}$$

585 Substituting Eq. (11) into Eq. (B.3) and only considering $0 \leq S \leq S_{max}$, Eq. (B.3) can be seen
586 to reduce to

$$\frac{\partial q_{ro}}{\partial S} = \frac{q_r - q_{in}}{S_{max}} < \frac{1}{\Delta t} \tag{B.5}$$

587 which, from further consideration of Eq. (11), shows that Eq. (B.1) will remain stable providing
588 that when $0 \leq S \leq S_{max}$, it is imposed that

$$q_{ro} < \frac{S}{\Delta t} \tag{B.6}$$

589 For the routing function, substituting Eq. (1) into Eq. (B.3), Eq. (B.4) can be seen to reduce to

$$abV^{b-1} < \frac{1}{\Delta t} \tag{B.7}$$

590 Stability for the routing function requires more careful consideration as compared to the soil
591 moisture accounting scheme because there is no natural upper limit for V (note that S_{max} is the
592 upper limit of S) and therefore V is unconstrained. However, to force the stability criterion in Eq.
593 (B.7) we can impose that $V < V_{max}$ where $V_{max} = (ab\Delta t)^{1/(1-b)}$, which is achieved as follows.

594 Consider the auxiliary variables, q_{trial} [L] and V_{trial} [L], found from:

$$q_{trial} = aV_n^b \tag{B.8}$$

$$V_{trial} = V_n + \Delta t(q_{ro,n} - q_{trial}) \tag{B.9}$$

595 The V_{max} constraint can be applied by calculating q_n and V_{n+1} from:

$$q_n = \begin{cases} q_{trial}, & V_{trial} < V_{max} \\ q_{ro,n} - \dfrac{(V_{max} - V_n)}{\Delta t}, & V_{trial} \geq V_{max} \end{cases} \tag{B.10}$$

$$V_{n+1} = \begin{cases} V_{trial}, & V_{trial} < V_{max} \\ V_{max}, & V_{trial} \geq V_{max} \end{cases} \tag{B.11}$$

596 In this way, stability is ensured by routing excess runoff direct to the catchment outlet during
597 exceptionally wet periods.

598 **Appendix C. Stability analysis for Euler explicit time-stepping schemes**

599 Consider a differential equation of the form

$$\frac{df}{dt} = -g \tag{C.1}$$

600 Applying an Euler explicit time-stepping scheme leads to a discrete solution of the form

$$f_{n+1} = f_n - \Delta t g_n \tag{C.2}$$

601 where $\Delta t = t_{n+1} - t_n$.

602 The approximate solution, $f(t_n) = f_n$, is related to the exact solution, f_0, by

$$f = f_0 + \epsilon \tag{C.3}$$

where ϵ is the error associated with the approximation.

Substituting Eq. (C.3) into Eq. (C.2) leads to

$$\frac{df_0}{dt} + \frac{d\epsilon}{dt} = -g(f_0 + \epsilon) \tag{C.4}$$

Applying a Taylor series expansion to $g(f_0 + \epsilon)$ then leads to

$$\frac{df_0}{dt} + \frac{d\epsilon}{dt} = -g(f_0) - \epsilon\frac{\partial g}{\partial f_0} + O(\epsilon^2) \tag{C.5}$$

Recalling that f_0 satisfies Eq. (C.1) exactly, Eq. (C.5) reduces to

$$\frac{d\epsilon}{dt} = -\epsilon\frac{\partial g}{\partial f_0} + O(\epsilon^2) \tag{C.6}$$

Applying the Euler explicit time-stepping scheme and rearranging then leads to

$$\frac{\epsilon_{n+1}}{\epsilon_n} = 1 - \Delta t\left[\frac{\partial g}{\partial f_0}\right]_n + O(\epsilon_n^2) \tag{C.7}$$

from which it can be understood that Eq. (C.2) will remain stable providing

$$\frac{\partial g}{\partial f} < \frac{1}{\Delta t} \tag{C.8}$$

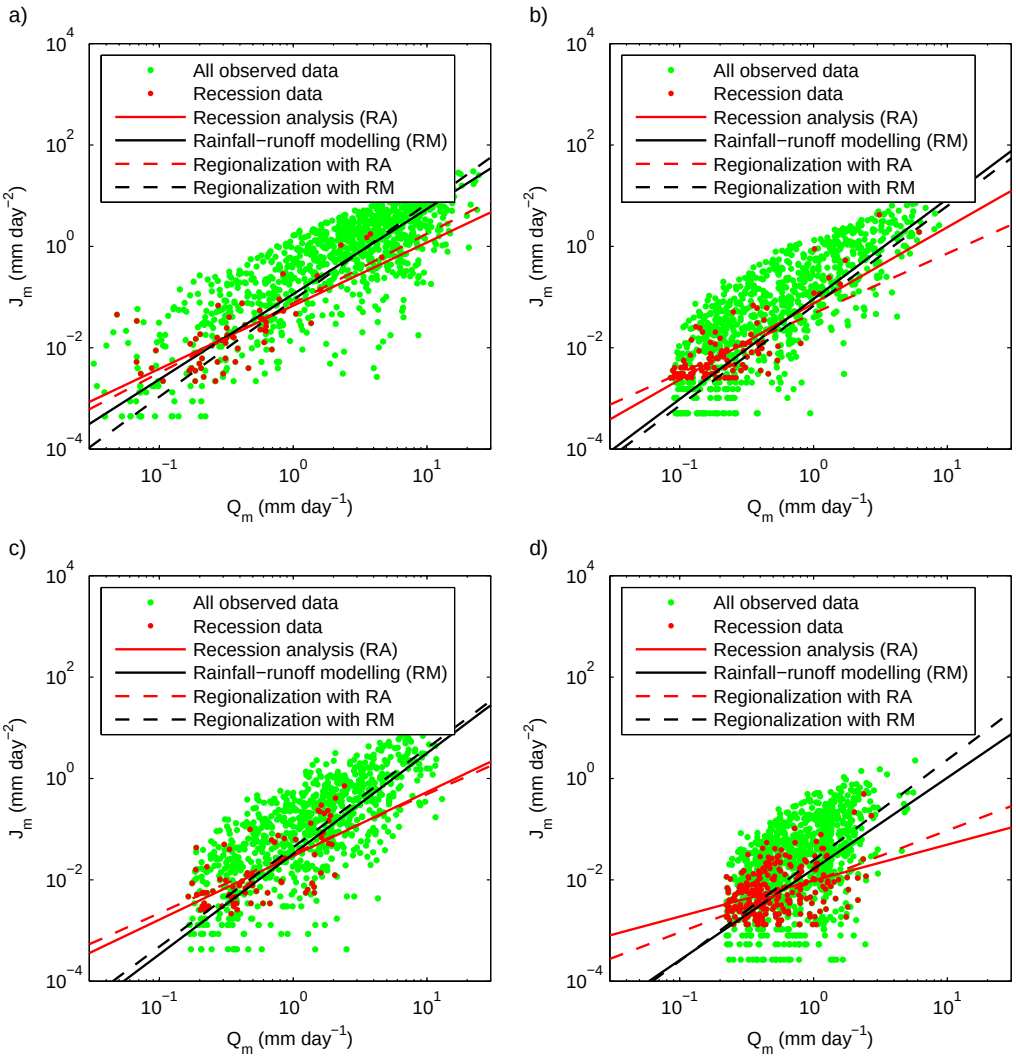

Figure 1: Plots of discharge rate gradient, J_m, against discharge rate, Q_m, for four selected catchments. The recession data represents a subset of the observed data where discharge rate is at least ten times larger than the precipitation minus the potential evapotranspiration. The red solid lines were obtained by regression analysis with the recession data, i.e., the recession analysis (RA). The red dashed lines were obtained by using regionalization equations (Eqs. (14) and (15)) derived from α and β parameters obtained by RA. The black solid lines were obtained by calibrating a rainfall-runoff model (RM). The black dashed lines were obtained by using regionalization equations (Eqs. (16) and (17)) derived from α and β parameters obtained from the RM calibration.

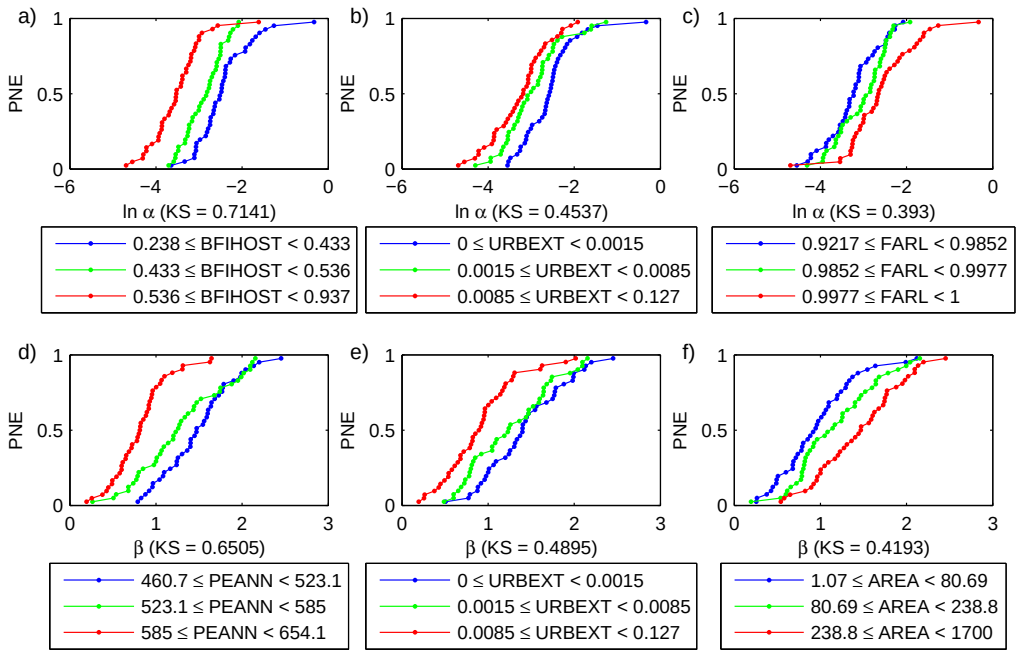

Figure 2: Cumulative distribution functions (CDF) for α and β, as obtained during the recession analysis, separated out in terms of the lower, middle and upper third ranges of the top three most sensitive catchment characteristics. PNE stands for probability of non-exceedance. The KS values reported alongside the x-axis labels denotes the Kolmogorov-Smirnov statistics between CDFs for the lower and upper thirds.

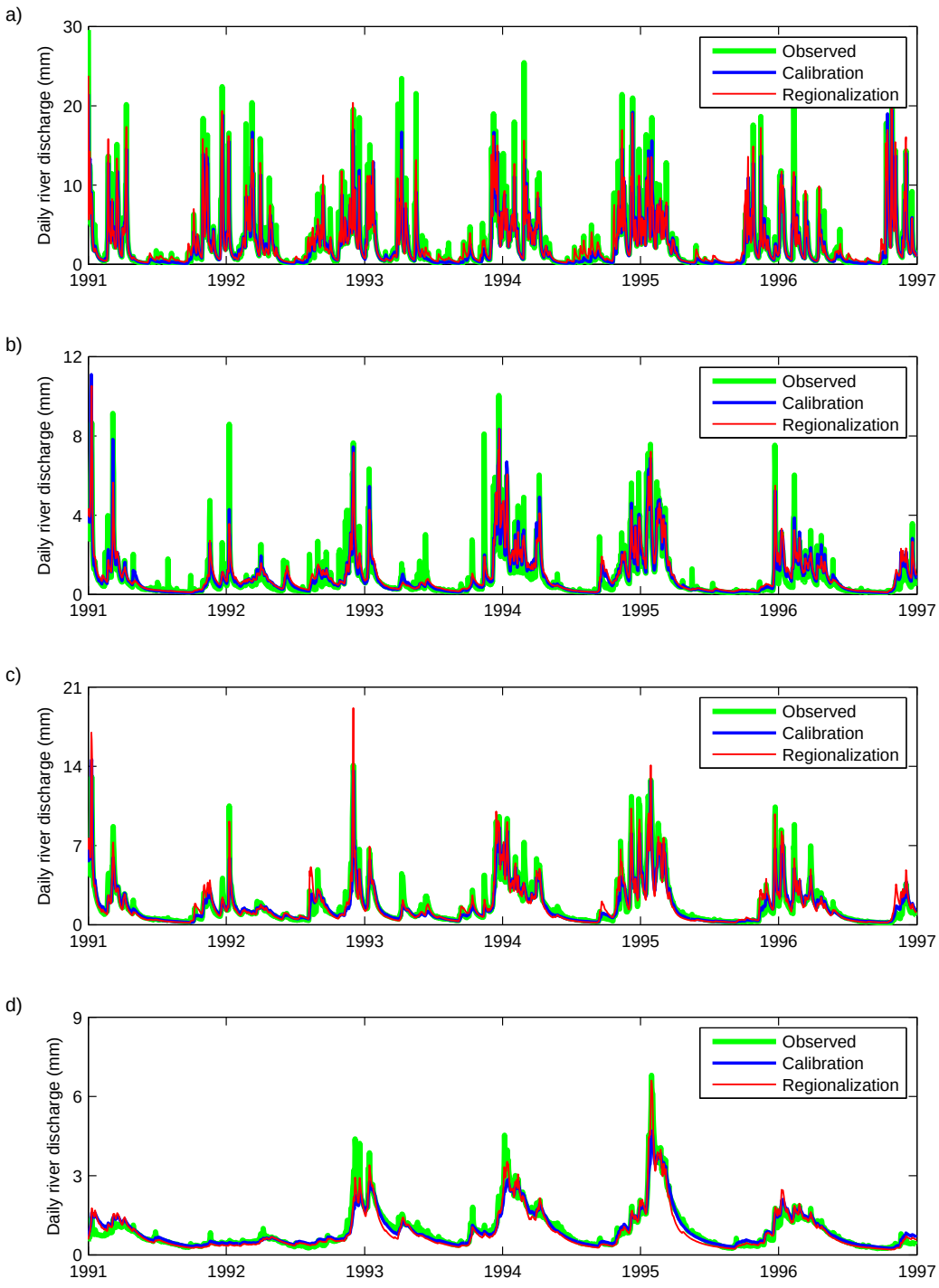

Figure 3: Plots of discharge rate against time during the validation period for the four selected catchments, previously presented in Fig. 1. The green lines are the observed discharge rate. The blue lines were obtained by calibrating the three parameter rainfall-runoff model to data from the calibration period (1981 to 1991). The red lines were obtained using the three parameter rainfall-runoff model in conjunction with the regionalization equations given in Eqs. (16) to (18).

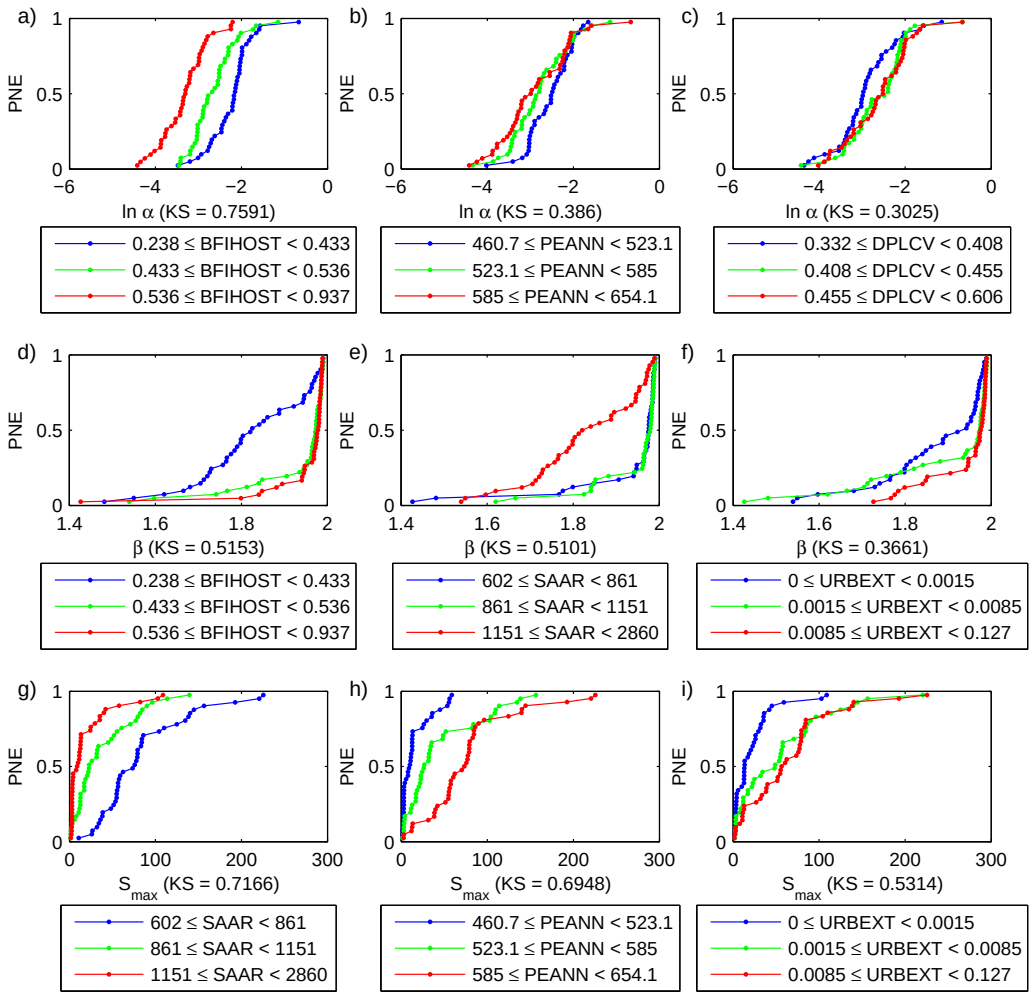

Figure 4: Cumulative distribution functions (CDF) for α, β and S_{max}, as obtained during the calibration of the rainfall-runoff model, separated out in terms of the lower, middle and upper third ranges of the top three most sensitive catchment characteristics. PNE stands for probability of non-exceedance. The KS values reported alongside the x-axis labels denotes the Kolmogorov-Smirnov statistics between CDFs for the lower and upper thirds.

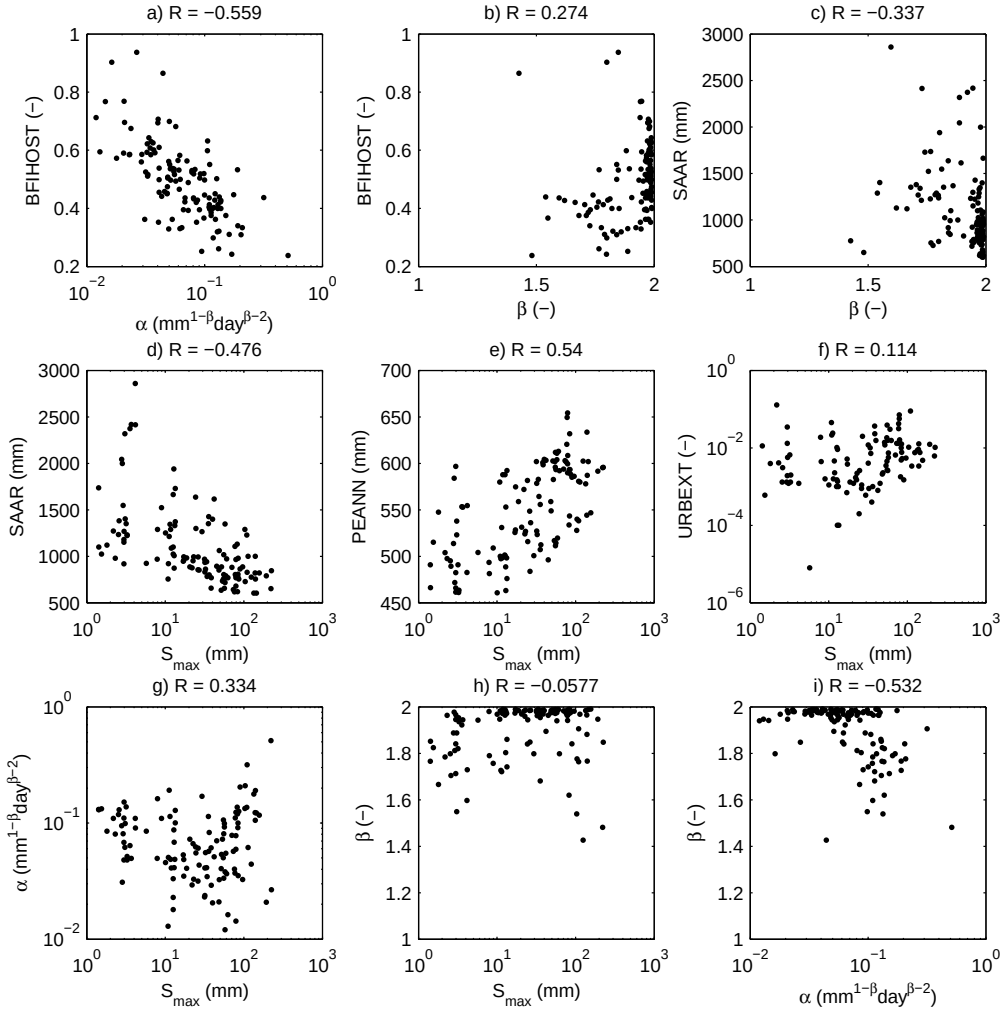

Figure 5: Univariate plots of calibrated rainfall-runoff model parameters plotted against themselves and other sensitive catchment characteristics. The *R* values denote the associated correlation coefficients.

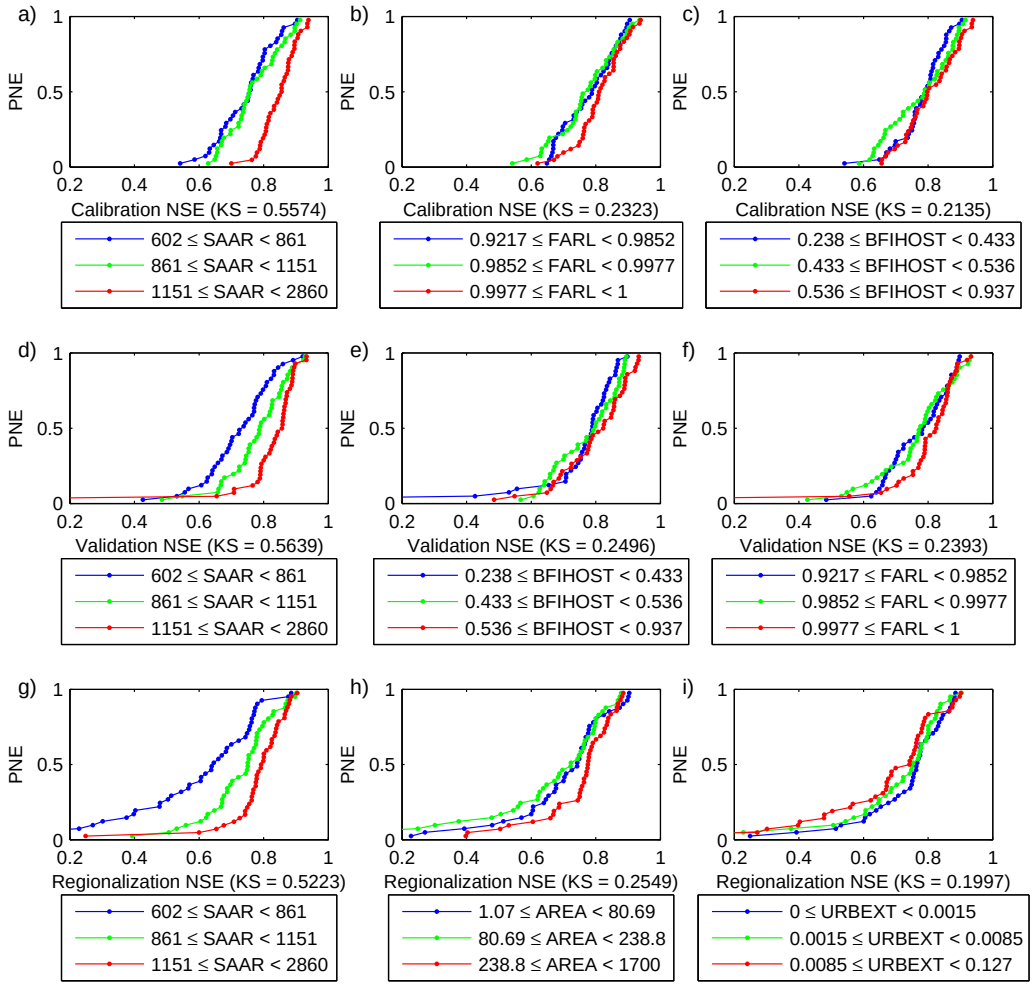

Figure 6: Cumulative distribution functions (CDF) for NSE values for the rainfall-runoff model, for the calibration period, the validation period and the validation period using the regionalization equations, separated out in terms of the lower, middle and upper third ranges of the top three most sensitive catchment characteristics. PNE stands for probability of non-exceedance. The KS values reported alongside the x-axis labels denotes the Kolmogorov-Smirnov statistics between CDFs for the lower and upper thirds.

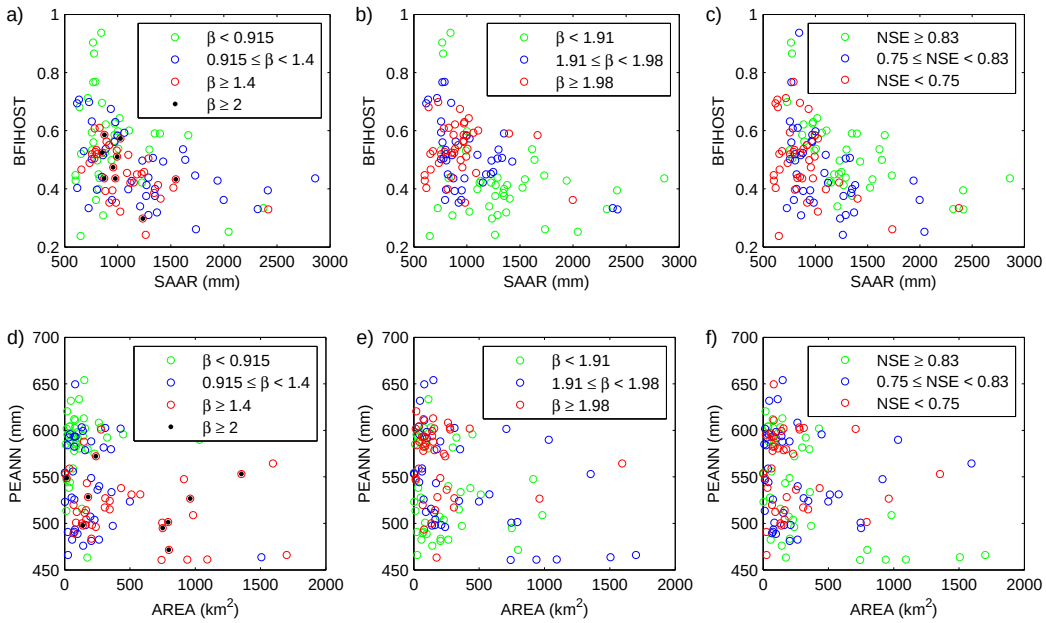

Figure 7: (a, b, c) Plots of BFIHOST against SAAR separated out in terms of the lower, middle and upper third ranges for: a) β as obtained from the recession analysis (RA); b) β as obtained from the rainfall-runoff modelling (RM) calibration; c) NSE values for the rainfall-runoff model during the validation period. (d, e, f) Plots of PEANN against AREA separated out in terms of the lower, middle and upper third ranges for: d) β as obtained from RA; e) β as obtained from the RM calibration; f) NSE values for RM during the validation period.